nature physics

Article

https://doi.org/10.1038/s41567-023-02320-z

Laser spectroscopy of a rovibrational transition in the molecular hydrogen ion H_2^+

Received: 14 June 2023

Accepted: 6 November 2023

Published online: 12 January 2024

Check for updates

M. R. Schenkel, S. Alighanbari & S. Schiller ✉

Comparison of precise predictions of the energy levels of the molecular hydrogen ion H_2^+—the simplest molecule—with measured vibrational transition frequencies would allow a direct determination of the proton-to-electron mass ratio and of the proton's charge radius. Here we report vibrational laser spectroscopy of trapped and sympathetically laser-cooled H_2^+, which represents a step towards this goal. We studied a first-overtone electric-quadrupole transition and measured its two hyperfine components. The determined spin-averaged vibrational transition frequency has a fractional uncertainty of 1.2×10^{-8} and is in agreement with the theoretically predicted value. We measured an analogous electric-quadrupole transition in HD^+ to estimate systematic uncertainties. Here, we observed a vastly improved line quality factor compared to previous electric-quadrupole spectroscopy of molecular ions. Our work demonstrates that first-overtone electric-quadrupole transitions are suitable for precision spectroscopy of molecular ions, including H_2^+, and that determining the proton-to-electron mass ratio with laser spectroscopy could become competitive with mass spectrometry using Penning traps. Furthermore, achieving precision spectroscopy of H_2^+ is an essential prerequisite for a future test of combined charge, parity and time reversal symmetry based on a comparison with its antimatter counterpart.

In recent years, it has been shown that the accurate determination of transition frequencies between rovibrational levels of molecular ions can contribute to current endeavours in fundamental physics. In particular, precision rotational and vibrational spectroscopy of the molecular hydrogen ion (MHI) HD^+ has allowed testing some predictions of quantum electrodynamics theory[1], determining a fundamental constant and searching for physics beyond the standard model[2–5]. For a discussion, see refs. 5–7. The heteronuclear HD^+ system is advantageous from an experimental point of view because it allows for electric-dipole (E1) transitions. Such transitions can be driven by moderate laser power. Also, any vibrational excitation decays on a timescale of tens of milliseconds to the ground vibrational level $v = 0$ by spontaneous emission (v is the vibrational quantum number). After thermalization with black-body radiation, an ensemble of HD^+ contains a sufficiently large fraction of molecules in any of a small set of rovibrational levels ($v = 0, N = 0, 1, 2, 3, 4$, where N is the rotational quantum number), a favourable situation. However, HD^+ also has shortcomings. First, it has a complex hyperfine structure (HFS), complicating experimentation and extraction of the spin-averaged (HFS-free) frequency, and second, the key properties of its two dissimilar nuclei, namely the mass and charge radius, cannot be independently deduced from spectroscopic data.

To overcome the latter, intrinsic limitation, there is a need to investigate at least one of the homonuclear MHIs, H_2^+ and D_2^+. Due to the smaller spin of the proton (1/2) compared to the deuteron (1), the HFS of H_2^+ is simpler and this molecule may be preferred. In homonuclear diatomics, E1 transitions between rovibrational levels in the same electronic state are forbidden. As a consequence, the natural lifetimes of excited vibrational levels are extremely long, of the order of 1 week for H_2^+ (ref. 8). Thus, homonuclear MHIs lack a natural vibrational state preparation: they do not readily decay to the vibrational ground state. Conversely, the natural linewidths of transitions between these levels are extremely small. This leads to the exciting perspective of

Institut für Experimentalphysik, Heinrich-Heine-Universität Düsseldorf, Düsseldorf, Germany. ✉e-mail: step.schiller@hhu.de

https://doi.org/10.1038/s41567-023-02320-z

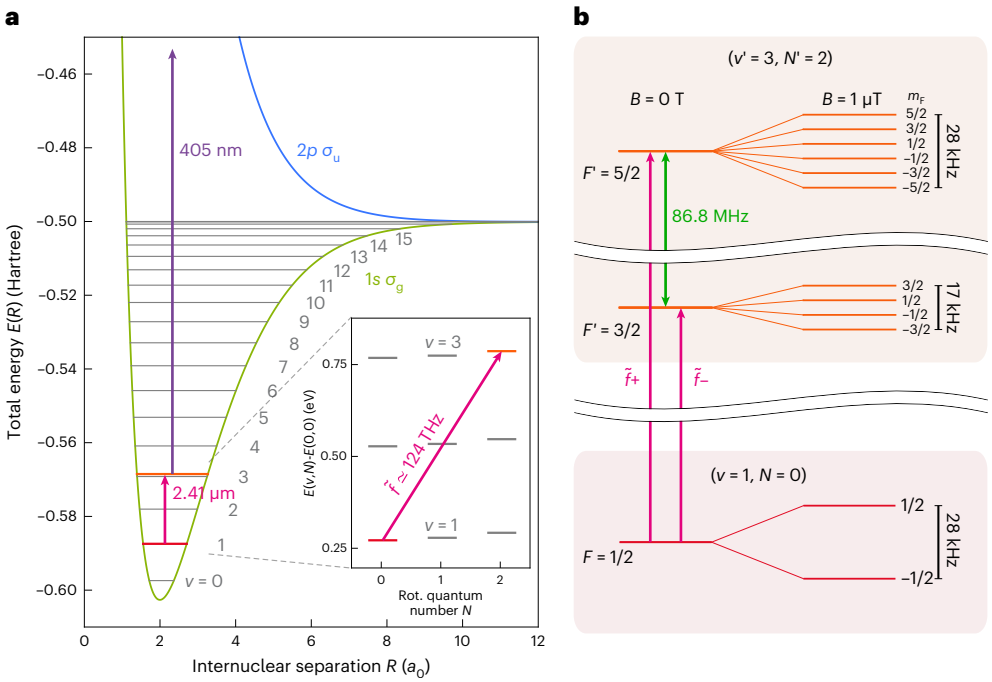

Fig. 1 | Energy levels of H_2^+ and transitions relevant to this work. a, H_2^+ molecular energy as a function of proton separation R in units of the Bohr radius a_0 for the two energetically lowest electronic states $1s\,\sigma_g$ and $2p\,\sigma_u$. The indicated vibrational energy levels (grey) are those for $N = 0$. The inset shows the first three rotational (Rot.) levels of the vibrational states $v = 1$–3. The studied transition $(v = 1, N = 0) \rightarrow (v' = 3, N' = 2)$ is shown by the magenta arrows. The dissociation laser's photon energy is indicated by the purple arrow. **b**, Hyperfine and Zeeman structure of the two rovibrational levels pertinent to the present study. The electron-spin-rotation coupling splits the upper vibrational level into two states $F' = 3/2$ and 5/2, separated by 86.8 MHz (green arrow). The magenta arrows indicate the measured hyperfine components $\tilde{f}_+$ and $\tilde{f}_-$. The Zeeman splittings in a finite magnetic field $B = 1\,\mu T$ are shown for illustration. During the exposure of the molecules to the spectroscopy wave, the magnetic field was substantially smaller. To show the Zeeman splittings, the vertical axis is broken at two positions. F is the total angular momentum of the molecule and m_F is the total angular momentum projection quantum number.

spectroscopy with extremely high line resolution, limited only by the spectral purity of the laser. Such performance would be important for implementing fundamental tests of physics, for which the highest frequency accuracy is desirable[9].

Furthermore, rovibrational transitions must be induced by two-photon[10] or electric-quadrupole (E2) excitation[11,12]. The squared Rabi frequency for E2 excitation in a homonuclear MHI is substantially smaller than for the E1 excitation of a comparable transition in a heteronuclear MHI (Methods), posing a challenge due to the requirement for high laser intensities. Note that E1 transitions in homonuclear MHI do exist because of the presence of spin interactions, but the transition strengths between low-lying vibrational levels are predicted to be orders of magnitude weaker than for E2 transitions[13].

Although H_2^+ has been investigated theoretically for almost a century[14,15], no direct measurements of the vibrational structure of H_2^+ near the bottom of the internuclear potential curve have ever been performed. A few spectroscopic studies of H_2^+ have addressed rovibrational states close to the dissociation limit of the electronic ground state. Two studies determined electronic transition frequencies, including rovibrational contributions, with 10^{-6}-level uncertainty[16,17]. A third study measured a pure rotational transition with 4×10^{-5} uncertainty[18]. An alternative approach of studying transitions in highly excited Rydberg states of neutral H_2 (refs. 19,20) yielded two rotational transitions with uncertainties $(3, 5) \times 10^{-7}$. There has been no improvement in accuracy or resolution since 1990.

E2 transitions in H_2^+, first discussed theoretically 70 years ago, have never been observed in absorption and have been observed only in spontaneous emission under extreme conditions[21]. In fact, there has so far been only a single study of E2 vibrational (laser) spectroscopy of molecular ions, on N_2^+ at 4.6 μm (ref. 22). Note that E2 spectroscopy of neutral H_2 is well developed[23–25], because these molecules are readily available at high density and absorption spectroscopy can be performed at easily available near-infrared laser wavelengths.

In this work, we perform vibrational laser spectroscopy of H_2^+, achieving a tenfold higher fractional accuracy than any other hitherto measured transition frequency of this molecule. We also present a precision study of E2 spectroscopy in a molecular-ion system to determine systematic shifts and explore its potential.

HFS of H_2^+

The rovibrational H_2^+ transition addressed in this work is illustrated in Fig. 1a. H_2^+ exhibits a HFS in all rovibrational levels, except when $N = 0$ (N is the rotational quantum number). In homonuclear diatomics, the HFS is simplified because of the anti-symmetrization principle for fermions. The total nuclear spin I takes on even or zero values in levels of even or zero N, the so-called para-levels. Thus, para-H_2^+ (that is, $N = 0, 2, 4, \ldots$) has $I = 0$. This leads to a very simple hyperfine Hamiltonian, containing only the interaction between electron spin and molecular rotation, $c_e(v, N)\,\mathbf{S}_e \cdot \mathbf{N}$. Here, c_e is the coupling coefficient, $\mathbf{S}_e$ is the electron spin operator and $\mathbf{N}$ is the rotational angular momentum operator. In contrast to the vibrational structure, the HFS of H_2^+ was measured a long time ago and accurately in levels $v = 4$–8, with uncertainties at the 1.5 kHz level, using radio-frequency (RF) spectroscopy[26]. After a half-century-long development, ab initio theory was able to match the experimental uncertainty[27–32].

The E2 transition with the simplest HFS is between levels with $N = 0$ and $N' = 2$ (or vice versa). We, therefore, chose to study this case, selecting $v = 1$ and $v' = 3$, as shown in Fig. 1b. The total angular momentum of the lower spectroscopy level ($v = 1, N = 0$) is $F = 1/2$, and there is no hyperfine splitting. For the upper spectroscopy level ($v' = 3, N' = 2$), angular momentum coupling yields $F' = 3/2$ or 5/2, and the level is split by the electron-spin-rotation interaction into two

https://doi.org/10.1038/s41567-023-02320-z

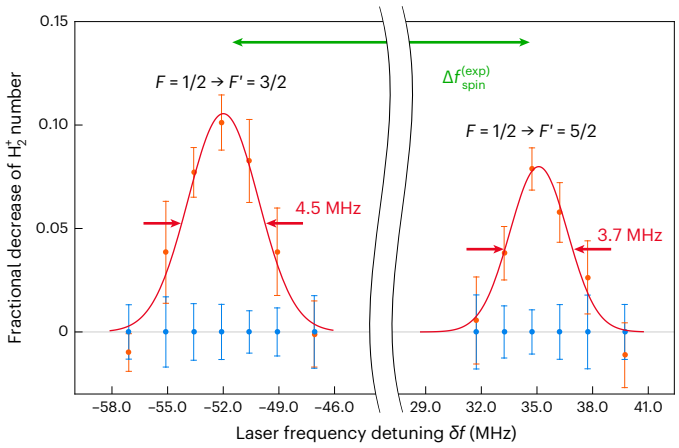

Fig. 2 | The two electron-spin-rotation components of the E2 rovibrational transition ($v = 1, N = 0$) → ($v' = 3, N' = 2$) in H_2^+. The laser frequency detuning δf is relative to the spin-averaged frequency $f_{spin\text{-}avg}^{(theor)} \approx 124$ THz. The red curves are guides for the eye. The horizontal axis is broken. The error bars are estimated standard errors of the means. The frequency errors are not shown because they are at a level of 10 Hz. F and F' are the total angular momentum quantum numbers of the initial and final states, respectively. The green arrow indicates the splitting of the two hyperfine components $\Delta f_{spin}^{(exp)}$. The measured linewidths (full-width at half-maximum) are shown as red arrows and labelled by their respective values.

non-degenerate states in absence of a magnetic field. One, therefore, expects two separate transitions: $\tilde{f}_-$: $(F = 1/2 \rightarrow F' = 3/2)$ and $\tilde{f}_+$: $(F = 1/2 \rightarrow F' = 5/2)$, since both satisfy the selection rules for E2 transitions.

Vibrational transition in H_2^+

To accomplish vibrational spectroscopy of H_2^+ and also obtain competitive accuracy, we trapped ensembles of molecules in a linear ion trap and sympathetically cooled them to millikelvin temperature using co-trapped laser-cooled beryllium ions[33]. An ensemble of H_2^+ was prepared from neutral para-H_2 gas leaked into the vacuum chamber and ionized by electron impact. This resulted in H_2^+ molecules being in a wide distribution of rovibrational levels[34]. Therefore, laser irradiation was applied to deplete the population in the upper spectroscopic level $(v' = 3, N' = 2)$ and in rovibrational levels with equal or larger v. A spectroscopy beam with a wavelength of 2.4 μm was aligned to the trap's symmetry axis. Repeated cycles of H_2^+ loading, preparation and spectroscopic excitation followed by dissociation were required to accumulate sufficient data to give spectroscopic lines (Methods and Extended Data Fig. 1). Our spectroscopy protocol gave Doppler-limited resolution. The spectroscopy wave was produced by a continuous-wave optical parametric oscillator (OPO) that provides sufficient power to drive the E2 transition. To permit accurate frequency measurements at 2.4 μm, we developed an optical frequency metrology system (Methods).

Figure 2 shows the measured hyperfine components of the vibrational transition. The full linewidths of ~4 MHz are due to Doppler broadening (see below). The transition frequencies are

$$\tilde{f}_-^{(exp)} = 124,486,979.9(2.3)\,\text{MHz},$$

$$\tilde{f}_+^{(exp)} = 124,487,066.7(1.9)\,\text{MHz}.$$

The lines exhibit low signal-to-noise ratios. We, therefore, assigned the line half-width at half-maxima as the statistical uncertainties of the frequencies.

Study of systematic effects

The systematic shifts of the H_2^+ transition could not be determined because the corresponding studies would have taken a prohibitively long time. The reason is the small fraction of molecules in the lower spectroscopy state obtained in each loading and purification cycle, leading to a low data acquisition rate. This also precluded attempting to search for Doppler-free transitions. To circumvent this difficulty, we instead studied in detail an E2 transition of the related heteronuclear HD^+, for which a sufficient data acquisition rate can be realized. We took advantage of the above-mentioned spontaneous decay of the molecular ion to $v = 0$ levels after ionization of the HD precursor and additionally applied laser rotational cooling[35] to transfer approximately 75% of the ions into the single rovibrational level ($v = 0, N = 0$). We, therefore, chose to study the $(v = 0, N = 0) \rightarrow (v' = 2, N' = 2)$ first-overtone E2 transition at $\lambda_2 = 2.6$ μm using the same OPO system. The quadrupole transition matrix element is a factor 2 smaller than for the studied transition in H_2^+ (Methods). The spectroscopy beam was aligned perpendicular to the trap axis.

As Fig. 3 shows, we observed ultra-narrow, Doppler-free resonances, as we observed for the fundamental transition $v = 0 \rightarrow v' = 1$ (ref. 4) and for the fourth-overtone transition $v = 0 \rightarrow v' = 5$ (ref. 5). Linewidths as low as ~40 Hz, that is line resolutions of 2.7×10^{12}, were achieved. This is a fourfold improvement compared to the best MHI E1 transition result (6×10^{11}; ref. 5) and is comparable to a recent molecular E2 transition measurement of the neutral diatomic Sr_2, which had a line resolution of 2.9×10^{12} (ref. 36). Moreover, it is an improvement by a factor of $\sim 10^6$ compared to the only previous study of a molecular-ion E2 transition[22]. The observed linewidths are due to a combination of the natural linewidth (5 Hz; ref. 37), power-broadening, short exposure, as well as the linewidth and frequency instability of the spectroscopy laser.

Table 1 summarizes the characterized shifts. The transition frequencies measured under nominal conditions must be corrected by approximately −1.2 kHz or -1×10^{-11} fractionally. The uncertainty of the corrections is 1×10^{-12} fractionally for one component and twice as large for the other because of its larger linewidth. Light shifts might occur due to off-resonant E1 coupling of the two spectroscopy levels by the intense spectroscopy wave, but we did not observe such an effect and a theoretical estimate gives a shift consistent with the non-observation. The two studied stretched-state Zeeman components have equal and opposite, purely linear Zeeman shifts. Therefore, the $B = 0$ extrapolated frequency of the HFS component is the mean of the two corrected frequencies. It has an uncertainty of 0.12 kHz or 1×10^{-12} fractionally.

Turning to H_2^+, notice that the Zeeman shifts of individual Zeeman components of a rovibrational transition are different from those in HD^+ (ref. 38). In the absence of a direct measurement, we rely on a theoretical prediction[39]. The H_2^+ Zeeman shifts of the various components $|\Delta m_F| \le 2$ of $\tilde{f}_+$ and $\tilde{f}_-$ are less than $|g_e \mu_B| \approx 28$ kHz μT^{-1} in magnitude (Methods and Extended Data Tables 1–3). During the H_2^+ spectroscopy intervals, we lowered the magnetic field to $|B| \le 0.2$ μT, so that the shifts were negligible compared to the linewidths. Any light shift due to off-resonant coupling by the spectroscopy wave should be negligible in H_2^+ due to the vanishing E1 transition moments between rovibrational states (Methods).

In view of these considerations, we deduced that in the H_2^+ experiment, systematic shifts were not relevant compared to the measurement resolution of 2 MHz. We estimated that power-broadening is not relevant (Methods), so that we associated the observed linewidths with an H_2^+ ensemble temperature $T \approx 3.4$ mK. In separate experiments on strings of HD^+ ions, we found temperatures of ≈1.5 mK. The higher value observed here could be due to the larger number of trapped H_2^+, resulting in a three-dimensional rather than string-like arrangement and less efficient sympathetic cooling.

Comparison of experimental and theoretical results and the proton-to-electron mass ratio

The spin-rotation coefficient was deduced to be $c_e(v' = 3, N' = 2) = 2(\tilde{f}_+ - \tilde{f}_-)/5 = 34.8(1.2)$ MHz, which is consistent with the most accurate theoretical prediction $c_e^{(theor)}(v' = 3, N' = 2) = 34.73025(12)$ MHz (ref. 32).

https://doi.org/10.1038/s41567-023-02320-z

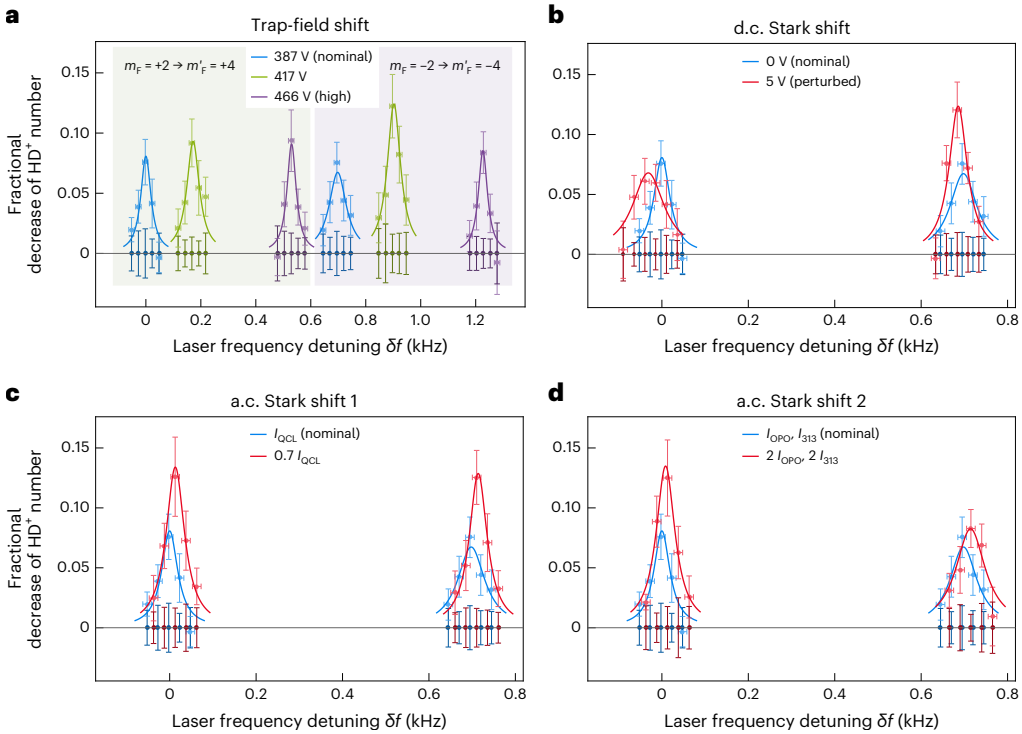

Fig. 3 | Two Zeeman components measured under different operating conditions. The two Zeeman components ($m_F = +2 \rightarrow m'_F = +4$) and ($m_F = -2 \rightarrow m'_F = -4$) of the hyperfine transition ($v = 0, N = 0, G_1 = 1, G_2 = 2, F = 2$) $\rightarrow$ ($v' = 2, N' = 2, G'_1 = 1, G'_2 = 2, F' = 4$) in HD^+, measured for a magnetic field strength of $B = 30$ μT. These are transitions between stretched spin states, that is states of maximum F and $|m_F|$. G_1 is the total spin of the proton–electron pair, and G_2 is the total particle spin, including also the deuteron. **a**, Each Zeeman component measured at trap-field amplitudes of 387, 417 and 466 V. The shaded regions group the same Zeeman component. **b**, Each Zeeman component measured at 0 and 5 V d.c. electric field. **c**, The a.c. Stark shift due to the quantum cascade laser (QCL) used for rotational cooling (Methods, 'HD$^+$ spectroscopy procedures') is studied by measuring the transitions at full (I_{QCL}) and 70% intensity. **d**, The a.c. Stark shift induced by the spectroscopy source and the cooling laser together, measured at nominal intensities (I_{OPO} and I_{313}, respectively) and doubled intensities. The lines measured under nominal conditions (blue points and blue curves) were measured once and are reproduced in each panel for illustration. The other points and corresponding curves in different colours are the lines measured under various conditions. The laser frequency detuning δf is relative to the optical frequency of the $m_F = +2 \rightarrow m'_F = +4$ component measured under nominal conditions. The coloured curves are guides for the eye. For display purposes, the data are divided into 25-Hz-wide bins and the average value of each bin is shown. The vertical error bars are standard error of the mean in the bin. The horizontal error bars are the frequency uncertainty of the spectroscopy laser stemming from its linewidth (Methods).

Our spin-averaged frequency is $f^{(\mathrm{exp})}_{\mathrm{spin\text{-}avg}} = (3\tilde{f}_+ + 2\tilde{f}_-)/5 = 124,487,032.7(1.5)$ MHz. This is a directly measured vibrational frequency in H_2^+. Remarkably, our value improves on the previous measurements of such a frequency by several orders of magnitude. The most accurate (indirect) measurement was performed by G. Herzberg and his team over half a century ago[40], using Rydberg series spectroscopy of neutral H_2 to obtain the first-overtone vibrational frequency with 7×10^{-5} uncertainty. With a fractional uncertainty of 1.2×10^{-8}, our value $f^{(\mathrm{exp})}_{\mathrm{spin\text{-}avg}}$ is now the most accurately measured property of H_2^+, including the HFS[26,41]. Note that the experimental uncertainty was too large to allow us to identify the presence or absence of a recoil shift (17.1 kHz).

The ab initio value for the frequency is $f^{(\mathrm{theor})}_{\mathrm{spin\text{-}avg}} = 124,487,032.45(6)$ MHz (Methods). The experimental and theoretical values agree.

The ab initio value requires as input the proton-to-electron mass ratio. This was taken from CODATA 2018. Instead, we can treat the mass ratio as an adjustable parameter in order to match the experiment with ab initio prediction, and obtain (Methods)

$$m_p/m_e = 1,836.152665(53).$$

The fractional uncertainty of this spectroscopically determined value (2.9×10^{-8}) is comparable to that which might be obtained from a comparison of experimental and theoretical results for the analogous transition in neutral H_2 (refs. 23,24). Note that the theoretical uncertainty of that transition[25] is twice as large as that quoted in refs. 23,24.

Outlook

A near-term goal of H_2^+ spectroscopy is to achieve a transition frequency uncertainty $u_{\mathrm{goal}} = u_r(f^{(\mathrm{exp})}_{\mathrm{spin\text{-}avg}}) \approx 2 \times 10^{-12}$, four times smaller than today's uncertainty for the quantum electrodynamics calculations (8×10^{-12}; ref. 1). This would lead to a theory-limited mass ratio uncertainty $u_r(m_p/m_e) \approx 1.8 \times 10^{-11}$. The present result obtained for an E2 transition of HD^+ indicates that the goal is realistic, provided that the Zeeman shifts can be controlled sufficiently well. For the present (or analogous) rovibrational transition, we have identified a suitable scheme (Extended Data Table 3). Four Zeeman components whose frequencies have pairwise opposite linear Zeeman shifts and tiny quadratic shifts can be combined to yield the spin-averaged frequency. The goal uncertainty u_{goal} is reached if each Zeeman component is measured with $u_r(f) \leq 4 \times 10^{-12}$ (0.5 kHz) total uncertainty. This requires a magnetic field stability $\delta B \approx 5 \times 10^{-2}$ μT (Methods), which is fulfilled with our apparatus. In the future, to achieve ultrahigh accuracy (10^{-16}-level uncertainty) in an RF trap, it appears more favourable to use a $(v, N = 2) \rightarrow (v', N' = 2)$ transition[42–45].

We briefly turn to the implications of this work for future vibrational spectroscopy of anti-H_2^+, which consists of two antiprotons bound by a positron and has never been observed. The spectroscopy would probe the charge and mass of the antiproton and of the positron as well as the antiproton–antiproton interaction and

Table 1 | Error budget of an E2 transition of HD^+

Effect	$f^{(exp)} - f^{(exp,nom)}$ (kHz)	
	$m_F = +2 \rightarrow m'_F = +4$	$m_F = -2 \rightarrow m'_F = -4$
Statistics	0.00(2)	0.00(6)
Trap field	−1.18(10)	−1.18(16)
a.c. Stark (OPO and 313 nm laser)	0.01(3)	0.00(8)
a.c. Stark (5.5 μm laser)	0.03(4)	0.00(7)
d.c. Stark	0.00(3)	0.00(9)
Total	−1.14(12)	−1.19(22)

Measured systematic shifts and their uncertainties are given for two Zeeman components of one HFS component of the first-overtone transition $(v = 0, N = 0) \rightarrow (v' = 2, N' = 2)$ at 115 THz. $f^{(exp)}$ is the extrapolated, unperturbed frequency. $f^{(exp,nom)}$ is the frequency under standard operating conditions. Here, m_F (m'_F) is the projection of the total angular momentum F (F') of the initial (final) state onto the direction of the static magnetic field. See Methods, 'Systematics of the HD^+ E2 transition', for a detailed discussion of these effects.

positron–antiproton interaction. A charge, parity and time reversal symmetry (CPT) test would compare the vibrational frequency of anti-H_2^+ with its matter counterpart. Such a test is attractive because (1) a potential ultrahigh accuracy (10^{-17} fractional uncertainty) may be reached, presumably exceeding the potential future performance of antiprotonic helium spectroscopy[46] and of antiproton mass spectrometry[47], (2) it also involves the antiproton–antiproton interaction, which does not occur in other accessible antiparticle-containing systems, and (3) it has a much higher sensitivity to the antiproton mass compared to anti-hydrogen, for which it is only a reduced-mass effect. Both anti-H_2^+ spectroscopy proposals[48,49] have considered E2 transitions and the non-destructive read-out of the internal molecular state in a cryogenic trap. Future anti-H_2^+ production methods[50] and established non-destructive interrogation methods may favour the use of Penning traps, which are already used for studying antiprotons. Note that vibrational transitions have Zeeman components that have particularly small and opposite linear Zeeman shifts in the strong magnetic field of a Penning trap (Methods), so that the corresponding uncertainties would be negligible, even during long-term measurements.

A CPT test can be extended to a local position invariance test by performing the anti-H_2^+ versus H_2^+ comparison over the course of a year, as the Earth moves around the Sun and probes a varying solar gravitational potential. Such a test would be similar to a local position invariance test that compares the mass-to-charge ratios of an antiproton and a negatively charged hydrogen ion H^- (ref. 47) but would be more accurate and more encompassing, given the presence of the antiproton–antiproton interaction in anti-H_2^+.

The present results are an important step towards turning H_2^+ into a second member of the MHI family accessible to the metrology of fundamental constants and, eventually, also D_2^+. The simplicity of removing the HFS effects to obtain the spin-averaged frequency will be an important advantage. Since the studied E2 transitions in both H_2^+ and HD^+ are not special cases, we believe that accurate E2 spectroscopy should be achievable with many homonuclear molecular-ion species. This underlines the potential of E2 spectroscopy of molecular ions aimed at testing for a possible time-variation of the electron-nuclear mass ratio[9,51,52].

Progress in H_2^+ and D_2^+ spectroscopy would be greatly facilitated if non-destructive internal state detection methods[53,54] and efficient state preparation that have been demonstrated for other species could be applied to these molecules. This will require measurements of single ions, which also promises higher accuracy. Concerning state preparation, spontaneous decay in a cryogenic Penning trap[21] and state-selective photoionization of H_2 (ref. 55) are demonstrated solutions. Recently, non-destructive, high-resolution electron-spin resonance spectroscopy of a single HD^+ molecule trapped for weeks in a Penning trap has been achieved[56], demonstrating both quantum-state identification and transition detection without molecule destruction. In an RF trap, the preparation of a single H_2^+ ion cooled by a single laser-cooled Be^+ ion to the motional ground state was demonstrated[57]. Together with the present result for the feasibility of high-accuracy E2 spectroscopy, these milestones give support to proposals for developing a CPT/local position invariance test based on comparing the vibrational transition frequencies of H_2^+ and anti-H_2^+.

Online content

Any methods, additional references, Nature Portfolio reporting summaries, source data, extended data, supplementary information, acknowledgements, peer review information; details of author contributions and competing interests; and statements of data and code availability are available at https://doi.org/10.1038/s41567-023-02320-z.

References

1. Korobov, V. I. & Karr, J.-P. Rovibrational spin-averaged transitions in the hydrogen molecular ions. *Phys. Rev. A* **104**, 032806 (2021).
2. Alighanbari, S., Giri, G. S., Constantin, F. L., Korobov, V. I. & Schiller, S. Precise test of quantum electrodynamics and determination of fundamental constants with HD^+ ions. *Nature* **581**, 152–158 (2020).
3. Patra, S. et al. Proton-electron mass ratio from laser spectroscopy of HD^+ at the part-per-trillion level. *Science* **369**, 1238–1241 (2020).
4. Kortunov, I. V. et al. Proton-electron mass ratio by high-resolution optical spectroscopy of ion ensembles in the resolved-carrier regime. *Nat. Phys.* **17**, 569–573 (2021).
5. Alighanbari, S., Kortunov, I. V., Giri, G. S. & Schiller, S. Test of charged baryon interaction with high-resolution vibrational spectroscopy of molecular hydrogen ions. *Nat. Phys.* **19**, 1263–1269 (2023).
6. Schiller, S. Precision spectroscopy of molecular hydrogen ions: an introduction. *Contemp. Phys.* **63**, 247–279 (2022).
7. Karr, J.-P. & Koelemeij, J. C. J. Extraction of spin-averaged rovibrational transition frequencies in HD^+ for the determination of fundamental constants. *Mol. Phys.* **121**, e2216081 (2023).
8. Bates, D. R. & Poots, G. Properties of the hydrogen molecular ion I: quadrupole transitions in the ground electronic state and dipole transitions of the isotopic ions. *Proc. Phys. Soc. Sect. A* **66**, 784–792 (1953).
9. Schiller, S. & Korobov, V. Test of time-dependence of the electron and nuclear masses with ultracold molecules. *Phys. Rev. A* **71**, 032505 (2005).
10. Karr, J.-P. et al. Vibrational spectroscopy of H_2^+: hyperfine structure of two-photon transitions. *Phys. Rev. A* **77**, 063410 (2008).
11. Korobov, V. I., Danev, P., Bakalov, D. & Schiller, S. Laser-stimulated electric quadrupole transitions in the molecular hydrogen ion H_2^+. *Phys. Rev. A* **97**, 032505 (2018).
12. Danev, P., Bakalov, D., Korobov, V. I. & Schiller, S. Hyperfine structure and electric quadrupole transitions in the deuterium molecular ion. *Phys. Rev. A* **103**, 012805 (2021).
13. Korobov, V. I. & Bakalov, D. Forbidden ortho–para electric dipole transitions in the H_2^+ ion. *Phys. Rev. A* **107**, 022812 (2023).
14. Burrau, Ø. Berechnung des Energiewertes des Wasserstoffmolekel-Ions (H_2^+) im Normalzustand. *Die Naturwiss.* **I.**, 16–17 (1927).
15. Teller, E. Über das Wasserstoffmolekülion. *Z. Phys.* **61**, 458–480 (1930).
16. Carrington, A. et al. Microwave electronic spectroscopy, electric field dissociation and photofragmentation of the H_2^+ ion. *J. Chem. Soc. Faraday Trans.* **89**, 603–614 (1993).

17. Carrington, A., Leach, C. A. & Viant, M. R. Nuclear hyperfine structure in the electronic millimetre wave spectrum of H_2^+. *Chem. Phys. Lett.* **206**, 77–82 (1993).
18. Critchley, A. D. J., Hughes, A. N. & McNab, I. R. Direct measurement of a pure rotation transition in H_2^+. *Phys. Rev. Lett.* **86**, 1725–1728 (2001).
19. Arcuni, P. W., Fu, Z. W. & Lundeen, S. R. Energy difference between the (v=0, R=1) and the (v=0, R=3) states of H_2^+, measured with interseries microwave spectroscopy of H_2 Rydberg states. *Phys. Rev. A* **42**, 6950–6953 (1990).
20. Haase, C., Beyer, M., Jungen, C. & Merkt, F. The fundamental rotational interval of para-H_2^+ by MQDT-assisted Rydberg spectroscopy of H_2. *J. Chem. Phys.* **142**, 064310 (2015).
21. Fink, D. J. & Myers, E. G. Deuteron-to-proton mass ratio from simultaneous measurement of the cyclotron frequencies of H_2^+ and D^+. *Phys. Rev. Lett.* **127**, 243001 (2021).
22. Germann, M., Tong, X. & Willitsch, S. Observation of dipole-forbidden transitions in sympathetically cooled, state-selected, homonuclear diatomic molecular ions. *Nat. Phys.* **10**, 820–824 (2014).
23. Fleurbaey, H., Koroleva, A. O., Kassi, S. & Campargue, A. The high-accuracy spectroscopy of H_2 rovibrational transitions in the (2-0) band near 1.2 µm. *Phys. Chem. Chem. Phys.* **25**, 14749–14756 (2023).
24. Cozijn, F. M. J., Diouf, M. L. & Ubachs, W. Lamb dip of a quadrupole transition in H_2. *Phys. Rev. Lett.* **131**, 073001 (2023).
25. Komasa, J. Energy levels of the hydrogen molecule from relativistic nonadiabatic calculations. In *Proc. International Conference on Precision Physics and Fundamental Physical Constants (FFK)* (eds Widmann, E. & Karshenboim, S.) Tu-4 (Stefan Meyer Institute for Subatomic Physics, 2023); indico.cern.ch/event/1164804/
26. Jefferts, K. B. Hyperfine structure in the molecular ion H_2^+. *Phys. Rev. Lett.* **23**, 1476–1478 (1969).
27. Somerville, W. B. A revised radio-frequency spectrum for H_2^+. *Mon. Not. R. Astron. Soc.* **147**, 201–205 (1970).
28. Kalaghan, P. & Dalgarno, A. Hyperfine structure of the molecular ion H_2^+. *Phys. Lett. A* **38**, 485–486 (1972).
29. McEachran, R., Veenstra, C. & Cohen, M. Hyperfine structure in the hydrogen molecular ion. *Chem. Phys. Lett.* **59**, 275–280 (1978).
30. Babb, J. F. & Dalgarno, A. Electron-nuclear coupling in the hyperfine structure of the hydrogen molecular ion. *Phys. Rev. Lett.* **66**, 880–882 (1991).
31. Babb, J. F. & Dalgarno, A. Spin coupling constants and hyperfine transition frequencies for the hydrogen molecular ion. *Phys. Rev. A* **46**, R5317–R5319 (1992).
32. Haidar, M., Korobov, V. I., Hilico, L. & Karr, J.-P. Higher-order corrections to spin–orbit and spin–spin tensor interactions in hydrogen molecular ions: theory and application to H_2^+. *Phys. Rev. A* **106**, 022816 (2022).
33. Blythe, P., Roth, B., Fröhlich, U., Wenz, H. & Schiller, S. Production of ultracold trapped molecular hydrogen ions. *Phys. Rev. Lett.* **95**, 183002 (2005).
34. Yang, W., Alheit, R. & Werth, G. Vibrational population of H_2^+ after electroionization of thermal H_2. *Z. Phys. D: At. Mol. Clusters* **28**, 87–88 (1993).
35. Schneider, T., Roth, B., Duncker, H., Ernsting, I. & Schiller, S. All-optical preparation of molecular ions in the rovibrational ground state. *Nat. Phys.* **6**, 275–278 (2010).
36. Leung, K. H. et al. Terahertz vibrational molecular clock with systematic uncertainty at the 10^{-14} level. *Phys. Rev. X* **13**, 011047 (2023).
37. Amitay, Z., Zajfman, D. & Forck, P. Rotational and vibrational lifetime of isotopically asymmetrized homonuclear diatomic molecular ions. *Phys. Rev. A* **50**, 2304–2308 (1994).
38. Bakalov, D., Korobov, V. & Schiller, S. Magnetic field effects in the transitions of the HD^+ molecular ion and precision spectroscopy. *J. Phys. B: At. Mol. Opt. Phys.* **44**, 025003 (2011).
39. Karr, J.-P., Korobov, V. I. & Hilico, L. Vibrational spectroscopy of H_2^+: Precise evaluation of the Zeeman effect. *Phys. Rev. A* **77**, 062507 (2008).
40. Herzberg, G. & Jungen, C. Rydberg series and ionization potential of the H_2 molecule. *J. Mol. Spectrosc.* **41**, 425–486 (1972).
41. Menasian, S. C. *High Resolution Study of the* $(F,F_2)=(3/2,1/2)\rightarrow(1/2,1/2)$ *HFS Transitions in Stored* H_2^+ *Molecular Ions*. PhD thesis, Univ. of Washington (1973).
42. Schiller, S., Bakalov, D. & Korobov, V. I. Simplest molecules as candidates for precise optical clocks. *Phys. Rev. Lett.* **113**, 023004 (2014).
43. Karr, J.-P. H_2^+ and HD^+: candidates for a molecular clock. *J. Mol. Spectrosc.* **300**, 37 – 43 (2014).
44. Karr, J.-P. et al. Hydrogen molecular ions: new schemes for metrology and fundamental physics tests. *J. Phys.: Conf. Ser.* **723**, 012048 (2016).
45. Schiller, S. & Korobov, V. I. Canceling spin-dependent contributions and systematic shifts in precision spectroscopy of molecular hydrogen ions. *Phys. Rev. A* **98**, 022511 (2018).
46. Hori, M. et al. Buffer-gas cooling of antiprotonic helium to 1.5 to 1.7 K, and antiproton-to-electron mass ratio. *Science* **354**, 610–614 (2016).
47. Borchert, M. J. et al. A 16-parts-per-trillion measurement of the antiproton-to-proton charge-mass ratio. *Nature* **601**, 53–57 (2022).
48. Dehmelt, H. Economic synthesis and precision spectroscopy of anti-molecular hydrogen ions in Paul trap. *Phys. Scr.* **T59**, 423 (1995).
49. Myers, E. G. CPT tests with the antihydrogen molecular ion. *Phys. Rev. A* **98**, 010101 (2018).
50. Zammit, M. C. et al. Laser-driven production of the antihydrogen molecular ion. *Phys. Rev. A* **100**, 042709 (2019).
51. Kajita, M., Gopakumar, G., Abe, M., Hada, M. & Keller, M. Test of m_p/m_e changes using vibrational transitions in N_2^+. *Phys. Rev. A* **89**, 032509 (2014).
52. Hanneke, D., Carollo, R. A. & Lane, D. A. High sensitivity to variation in the proton-to-electron mass ratio in O_2^+. *Phys. Rev. A* **94**, 050101 (2016).
53. Wolf, F. et al. Non-destructive state detection for quantum logic spectroscopy of molecular ions. *Nature* **530**, 457–460 (2016).
54. Egl, A. et al. Application of the continuous Stern–Gerlach effect for laser spectroscopy of the $^{40}Ar^{13+}$ fine structure in a Penning trap. *Phys. Rev. Lett.* **123**, 123001 (2019).
55. Schmidt, J. et al. Trapping, cooling, and photodissociation analysis of state-selected H_2^+ ions produced by (3+1) multiphoton ionization. *Phys. Rev. Appl.* **14**, 024053 (2020).
56. König, C. M. et al. Hyperfine spectroscopy of single molecular hydrogen ions in a Penning trap at ALPHATRAP. In *Proc. International Conference on Precision Physics of Simple Atomic Systems* (eds Pachucki, K., Karshenboim, S. & Tong, X.) 14 (PSAS, 2022); psas.fuw.edu.pl/program/
57. Schwegler, N. et al. Trapping and ground-state cooling of a single H_2^+. *Phys. Rev. Lett.* **131**, 133003 (2023).

Methods

Details of the experiment

H_2^+ spectroscopy procedures. The experimental apparatus is the same we have used in our previous experiments[4,5]. We employ a modified spectroscopy scheme that allows us to perform spectroscopy of H_2^+ without requiring rotational state preparation.

First, the spectroscopy laser frequency is set to a desired value. One cycle (Extended Data Fig. 1) then starts by loading an ensemble of H_2^+ ions by electron impact ionization from a reservoir of para-H_2 admitted into the vacuum chamber by a leak valve. This is followed by depleting the population in levels with $v \geq 2$, including the upper spectroscopy level $(v' = 3, N' = 2)$, by performing photodissociation with two continuous-wave lasers at wavelengths of 313 and 405 nm. Since for both wavelengths the photodissociation cross section decreases strongly with decreasing v (ref. 58), the dissociation of molecules in $v = 1$ is negligible. After a subsequent determination of the number of trapped H_2^+ (see below), the vibrational transition $(v = 1, N = 0) \rightarrow (v' = 3, N' = 2)$ is excited and detected using resonance-enhanced multi-photon dissociation (REMPD), which has two steps: (1) excitation of the spectroscopy transition with the OPO radiation and (2) dissociation of the molecule from the upper spectroscopy level with the 405 nm laser (50 mW and intensity 25 W cm^{-2}). To avoid a light shift induced by the dissociation laser, an interleaved shuttering scheme was employed to prevent the simultaneous exposure of the ions to both lasers. Completing the cycle, the number of still trapped H_2^+ is determined.

In the following cycle, the background is measured (blue data points in Fig. 2). All settings are unchanged except that the OPO beam remains blocked. These alternating spectroscopy and background cycles are repeated many times until satisfactory statistics is accumulated. After completing each cycle, the ion cluster is purged from any ions other than Be^+ and a new H_2^+ ensemble is loaded so that there is a sufficient population in the lower spectroscopy level. During the REMPD intervals of both signal cycles and background cycles, we applied a magnetic field of $B = 0.0(2)$ μT, whereas at all other times the magnetic field was set to $B_{\mathrm{cooling}} \approx 45$ μT. To acquire a spectroscopic line, we set the OPO frequency to a range of values.

The spectroscopy signal was obtained by comparing the number of trapped H_2^+ ions before and after the REMPD. The signal was computed as the normalized decrease of the number of trapped ions $(N_\mathrm{i} - N_\mathrm{f})/(N_\mathrm{i} - N_\mathrm{b})$, where N_i and N_f are the initial and final fluorescence peak strengths of the secular excitation signal of H_2^+, respectively, and N_b is the background level of fluorescence without any secular excitation. To determine the number of trapped H_2^+ ions, the transverse secular motion excitation spectrum was recorded over the range 450–1,250 kHz. The resonance frequency of H_2^+ under nominal conditions was approximately 1,000 kHz. The spectrum was fitted by two Gaussian functions. The peak strength of the H_2^+ signal, which is proportional to the number of trapped H_2^+ ions, was then determined. This approach differs from our previous ones for which we usually resonantly excited the secular motion at fixed frequency and did not record a spectrum. Here, the different approach is necessary because chemical reactions generate H_3^+ ions in the trap, and their presence modifies the Coulomb interactions within the cluster and, thus, also modifies the secular frequency of the H_2^+ ensemble.

HD^+ spectroscopy procedures. HD^+ ions are prepared in a string arrangement. The spectroscopy wave was aligned perpendicular to the string, allowing us to obtain Doppler-free resonances. The $v = 0$ rotational state preparation was implemented by a quantum cascade laser tuned to the $(v = 0, N = 2) \rightarrow (v' = 1, N' = 1)$ transition (5.5 μm). The REMPD scheme comprises three excitations: the spectroscopy transition $(v = 0, N = 0) \rightarrow (v' = 2, N' = 2)$, a subsequent vibrational excitation $(v' = 2, N' = 2) \rightarrow (v'' = 6, N'' = 3)$ (1.56 μm) and finally photodissociation by a 266 nm wave. The second excitation enhances the dissociation rate because the photodissociation cross section of the level $(v' = 2, N' = 2)$ is small at 266 nm.

The spectroscopy cycle sequence is the same as in refs. 4,5, except that the REMPD duration was increased to 30 s. We mention only the main aspects here. The spectroscopy wave was interleaved with the other two waves to avoid systematic shifts. Before and after REMPD the secular motion of HD^+ was resonantly excited to determine their number. Signal and background data were taken during alternating cycles. The cycles differ only in that the spectroscopy wave was kept blocked during the background cycle. On average, five signal and background cycle pairs can be executed before the HD^+ population has declined substantially. Once this has occurred, the Be^+ ion cluster is cleaned. That is, any ions other than beryllium are removed, and a fresh string of HD^+ ions is prepared. The quantum cascade laser was kept on during REMPD.

Spectroscopy laser system. The spectroscopy laser system is a continuous-wave OPO with an output power of >2 W at the H_2^+ and HD^+ transition wavelengths of 2.4 and 2.6 μm, respectively. The OPO wave was frequency-doubled to a second-harmonic wave that is suitable for generating a heterodyne beat with an erbium-fibre frequency comb. The second-harmonic wave was phase-locked to a comb line using this beat and feedback control to the OPO pump laser frequency. This effectively also locked the frequency of the spectroscopy wave to the comb.

To ensure the ultra-narrow linewidth of the spectroscopy radiation, the comb was optically stabilized by phase-locking to a near-infrared laser that is frequency-locked to a high-finesse resonator. Through a second beat with an independently optically stabilized frequency comb, we determined that the fractional frequency instability (Allan deviation) of the OPO spectroscopy wave frequency is below 1×10^{-13} for integration times longer than 1 s. An upper bound for the linewidth of the OPO radiation was obtained from an analysis of the beat. On the 5 s timescale, it was 10 Hz (full-width at half-maximum of a Lorentzian fit). This is also the main contribution to the OPO frequency uncertainty and as such determines the horizontal error bars shown in Fig. 3. Both combs were referenced to an active hydrogen maser, whose properties were characterized (Methods, 'Maser shift').

E2 transitions of H_2^+ and HD^+

E2 in H_2^+. The E2 reduced transition matrix element of the studied first-overtone transition is $Q_0 = Q_{H_2^+}(v = 1, N = 0 \rightarrow v' = 3, N' = 2) = -0.053268$ atomic units[11]. Note that Q_0 is larger by almost a factor of 2 compared to the first overtone starting from $v = 0$: $Q_{H_2^+}(v = 0, N = 0 \rightarrow v' = 2, N' = 2) = -0.028919$ atomic units[11]. However, Q_0 is smaller by a factor of 9 compared to the fundamental vibrational transition starting from the same lower level $(v = 1, N = 0 \rightarrow v' = 2, N' = 2)$. Our spectroscopy source has adequate power to compensate for this difference.

For the upper rovibrational level, the Einstein coefficient for spontaneous emission was computed as $A_{H_2^+}(v' = 3, N' = 2 \rightarrow v = 1, N = 0) \approx 7.8 \times 10^{-8}$ s^{-1} (refs. 11,59).

E2 in HD^+. E2 transitions in this heteronuclear molecule have been discussed in refs. 45,60. The E2 reduced transition matrix element is $Q_{HD^+}(v = 0, N = 0 \rightarrow v' = 2, N' = 2) = 0.025976$ atomic units. The reduced electric-dipole (E1) transition matrix elements for near-by transitions are 0.00436 for the $(v = 0, N = 0) \rightarrow (2, 1)$ transition and −0.00609 for the $(v = 0, N = 1) \rightarrow (2, 2)$ transition, in atomic units[61]. Thus, the Rabi frequencies for these E1 transitions are approximately one order larger than for the studied E2 transition of HD^+.

Power-broadening. The Rabi frequency for an E2 transition in H_2^+ can be estimated using equation (15) of ref. 11. Using the E2 transition matrix element Q_0 and considering the peak intensity of the spectroscopy wave (3.6 MW m^{-2}), we estimated an upper limit for the Rabi frequency to be $\Omega/(2\pi) \approx 0.5$ kHz. Therefore, power-broadening is negligible compared to the observed linewidth.

The Rabi frequency for an E2 transition in HD^+ between stretched states can be obtained from the same equation. The peak intensity in the E2 spectroscopy of HD^+ was 2.6 MW m^{-2}. Taking into account the angle between the magnetic field and the wavevector and its uncertainty, we estimated the Rabi frequency to be $\Omega/(2\pi) \leq 15$ Hz, consistent with the observed linewidths.

Systematics of the HD^+ E2 transition

Zeeman shift. See Fig. 3, all panels. The magnetic field in our trap was characterized by stimulated Raman spectroscopy to precisely measure the Zeeman splitting of beryllium ions[62] and, by comparison, of the observed and calculated Zeeman splittings of the fundamental rotational transition[2]. Comparing the measured Zeeman splitting of the two components, 0.72(7) kHz, with the theoretical prediction, equation (6) in ref. 38, we deduced a magnetic field strength of 30 μT, consistent with the previous determinations for the same coil current settings.

Trap-field-induced shift. The RF electric field in the trap induces a shift, which was determined for both Zeeman components at nominal magnetic field (Fig. 3a). Measurements at three different RF amplitudes and extrapolation to zero amplitude indicate that there was a systematic shift of approximately +1.2 kHz for both components under the nominal operating conditions. This type of shift was observed by us earlier[2]; for a recent investigation of a different molecular ion, see ref. 63.

a.c. and d.c. Stark shifts. The beryllium ion cooling laser, the spectroscopy wave and the rotational cooling laser potentially cause a.c. Stark shifts (Fig. 3c–d). We measured the transition frequencies at different laser wave powers but did not resolve any light shift induced by these waves.

Also, we could not resolve any d.c. Stark shift upon comparing the transition frequencies measured under the nominal conditions and for an additional d.c. voltage of 5 V applied to two trap electrodes (Fig. 3b).

Maser shift. All frequencies used for the HD^+ measurements were corrected for the hydrogen maser frequency offset. The offset was determined by continuously comparing the maser frequency to an atomic time signal provided by a global navigation satellite system at 1 pulse per second. The fractional offset from the atomic frequency and the fractional drift were found to be $\approx 8 \times 10^{-12}$ and $\approx 1 \times 10^{-13}$ per month, respectively. Since the spectroscopy measurements were taken over 2 months, the laser frequencies obtained on a particular measurement day were corrected for the offset on that day.

Systematics of the H_2^+ E2 transitions

Theory of Zeeman shifts. The Zeeman shifts in a weak field are discussed in refs. 44,45 for $N = 0 \rightarrow N' = 2$ transitions, and in refs. 42,43,45 for $N = 2 \rightarrow N' = 2$ transitions. For a strong field, ref. 49 gives a partial discussion of a $N = 2 \rightarrow N' = 2$ transition.

For completeness, we present in Extended Data Table 1 the Hamiltonians $H_{spin}(N) + H_{Zeeman}(N)$ for $N = 2$ and for the trivial case $N = 0$. The $N = 2$ case uses the approximation of isotropic electronic g factor; for the calculation of the anisotropy, see refs. 64,65.

Note that the electronic g factor $g_e(v, N)$ (refs. 64,65), the rotational g factor $g_i(v, N)$[39] and the spin-rotation coupling constant $c_e(v, N)$ (ref. 32) depend on the rovibrational level. Because the dependencies are weak, there are rovibrational transitions with low magnetic sensitivity. In addition, by measuring two or more Zeeman components and suitably averaging them, the net Zeeman shift can be made to cancel.

From the Hamiltonians, one can compute the Zeeman shifts for transitions of the type $(v, N = 0) \rightarrow (v', N' = 2)$, $(v, N = 2) \rightarrow (v', N' = 0)$ and $(v, N = 2) \rightarrow (v', N' = 2)$ for arbitrary field strength and perform series expansions in the low-field limit (for RF traps) and in the high-field limit (for Penning traps). These lead to the expressions in Extended Data Table 2.

The predicted frequencies of a few selected HFS components of the transition studied in the present work are displayed in Extended Data Table 3. The magnitude of the linear Zeeman shift of the components $f_b^{(\pm)}$, ±5.6 kHz × B/μT, determines an upper limit for the allowable instability of the magnetic field, δB, for a desired total uncertainty.

Next, we mention some examples of interesting transitions in a Penning trap. The two Zeeman components ($v = 0, N = 2, m_s = \pm 1/2, m_F = \pm 1/2$) → ($v' = 1, N' = 2, m_s = \pm 1/2, m_F = \pm 1/2$) have sensitivities of ±8.2 kHz T^{-1} at $B = 4$ T. The two Zeeman components ($v = 0, N = 0, m_s = \pm 1/2, m_F = \pm 1/2$) → ($v' = 1, N' = 2, m_s = \pm 1/2, m_F = \pm 1/2$) have sensitivities of ±3.6 kHz T^{-1} at $B = 4$ T. These values are even lower than for the Zeeman component discussed in ref. 49, namely 150 kHz T^{-1}. The values of v and v' were chosen for comparison with that reference, but similar results hold also for other transitions.

Light shifts. A potential light shift from the 405 nm photodissociation laser is prevented by using appropriate interleaved shuttering.

The light shift due to the beryllium cooling wave (313 nm) and the OPO radiation can be estimated using a comparison with HD^+, for which it was determined to be less than 0.1 kHz.

Our analysis is based on ref. 66. For the transition in HD^+, the frequency-dependent polarizabilities should be considered. At 2.6 μm, the differential scalar polarizability is $\alpha_s(v' = 2, N' = 2) - \alpha_s(v = 0, N = 0) \approx 1.5$ atomic units. The tensor polarizability is estimated as $\alpha_t(v' = 2, N' = 2) = -0.1$ atomic units (it is zero when $N = 0$). This is to be multiplied by a Zeeman-state-dependent factor, which for the two addressed (pure) Zeeman states is 12.3. The maximum polarizability of the transition is, therefore, approximately 2.3 atomic units.

For the 2.4 μm radiation interrogating H_2^+, the light shift is essentially determined by the static polarizabilities, because the E1 transition dipole moments between rovibrational levels of the electronic ground state are effectively zero and because the spectroscopy wave photon energy is small compared to the excitation energy to higher electronic states. For the scalar polarizability, $\alpha_s(v' = 3, N' = 2) - \alpha_s(v = 1, N = 0) = 2.1$ atomic units. The tensor polarizability is $\alpha_t(v' = 3, N' = 2) = -0.53$ atomic units. This is again to be multiplied by a Zeeman-state-dependent factor. The largest factors for the two studied transitions (which contain all m_F' values) are 21/5 for the $F' = 3/2$ multiplet and 6 for the $F' = 5/2$ multiplet. The maximum polarizability of any Zeeman component of the transition is, therefore, approximately 3.2 atomic units. This value is close to that for the HD^+ case, and therefore, we may infer that the light shift from the OPO radiation is negligible in the present H_2^+ measurement and that it should be controllable at the 1×10^{-12} level in a next-generation experiment.

For the wavelength 313 nm, the differential polarizabilities are close to those at the spectroscopy wavelengths. Because of the much lower intensity of the 313 nm radiation, the corresponding light shift is negligible in comparison.

Other shifts. We have not measured the black-body shift of either HD^+ or H_2^+, but theory[66] predicts it to be at the 1×10^{-17} level for the present H_2^+ transition at room temperature.

We hypothesize that the trap shift that we observed for HD^+ for various transitions[2,4,5], including for the present one, may in part be due to off-resonant electric-dipole coupling to close rovibrational levels (a quasi-static Stark shift). Since E1 couplings between rovibrational levels in the ground electronic state are negligible in H_2^+, the trap shift could be smaller than in HD^+. Relevant static Stark shift coefficients for H_2^+ are discussed above.

Ab initio theory of $f_{spin\text{-}avg}$

The computation of the spin-averaged frequency follows ref. 67. CODATA 2018 recommended values for fundamental constants are used. The transition frequency is computed as a power series in the

fine-structure constant α. Considering the present experimental accuracy, only the major contributions need to be included:

$$\begin{aligned} f_{\text{spin-avg}} &= 124,485,554.55\,\text{MHz} \quad (\text{nonrelativistic}) \\ &+ 2,002.70\,\text{MHz} \quad (\alpha^2\ \text{order}) \\ &- 521.35\,\text{MHz} \quad (\alpha^3\ \text{order}) \\ &- 3.69\,\text{MHz} \quad (\alpha^4\ \text{order}) \\ &+ 0.24(6)\,\text{MHz} \quad (\alpha^5\ \text{order}) \\ &= 124,487,032.45(6)\,\text{MHz}. \quad (\text{total}) \end{aligned}$$

The orders are relative to the non-relativistic contribution. The α^5 contribution is a simple estimate based on ref. 67. Once the need arises, this contribution can be computed accurately and so can contributions of higher order. The sensitivity of the spin-averaged frequency to m_p/m_e is computed by solving the non-relativistic Schrödinger equation for two different values of m_p/m_e. We find $\partial f_{\text{spin-avg}}/\partial(m_p/m_e) = -0.43976 \times f_{\text{spin-avg}}/(m_p/m_e)$.

Data availability

Source data are provided with this paper. All other data that support the plots within this paper and other findings of this study are available from the corresponding author upon reasonable request.

Code availability

No custom code or software was used for analysing or presenting the data associated with this paper.

References

58. Dunn, G. H. Photodissociation of H_2^+ and D_2^+: Theory. *Phys. Rev.* **172**, 1-7 (1968).
59. Olivares Pilón, H. & Baye, D. Quadrupole transitions in the bound rotational-vibrational spectrum of the hydrogen molecular ion. *J. Phys. B: At. Mol. Opt. Phys.* **45**, 065101 (2012).
60. Bekbaev, A. K., Aznabayev, D. T. & Korobov, I. V. Quadrupole transitions of the hydrogen molecular ion HD^+. In *Proc. International Conference on Precision Physics and Fundamental Physical Constants* Vol. 9 (eds Horváth, D., Karshenboim, S. & Siklér, F.) 058 (2019).
61. Bakalov, D. & Schiller, S. Static Stark effect in the molecular ion HD^+. *Hyperfine Interact.* **210**, 25–31 (2012).
62. Shen, J., Borodin, A. & Schiller, S. A simple method for characterization of the magnetic field in an ion trap using Be^+ ions. *Eur. Phys. J. D* **68**, 359 (2014).
63. Collopy, A. L., Schmidt, J., Leibfried, D., Leibrandt, D. R. & Chou, C.-W. Effects of an oscillating electric field on and dipole moment measurement of a single molecular ion. *Phys. Rev. Lett.* **130**, 223201 (2023).
64. Hegstrom, R. A. *g* factors and related magnetic properties of molecules. Formulation of theory and calculations for H_2^+, HD^+, and D_2^+. *Phys. Rev. A* **19**, 17–30 (1979).
65. Karr, J.-P. Leading-order relativistic corrections to the *g* factor of H_2^+. *Phys. Rev. A* **104**, 032822 (2021).
66. Schiller, S., Bakalov, D., Bekbaev, A. K. & Korobov, V. I. Static and dynamic polarizability and the Stark and blackbody-radiation frequency shifts of the molecular hydrogen ions H_2^+, HD^+, and H_2^+. *Phys. Rev. A* **89**, 052521 (2014).
67. Korobov, V. I., Hilico, L. & Karr, J.-P. Fundamental transitions and ionization energies of the hydrogen molecular ions with few ppt uncertainty. *Phys. Rev. Lett.* **118**, 233001 (2017).

Acknowledgements

We are indebted to V. I. Korobov for putting at our disposal his codes for the computation of the H_2^+ properties and for many important communications on the properties of MHI. We are grateful to S. Schlemmer (Universität zu Köln) for generously providing para-H_2 gas. G. S. Giri contributed to early tests of the spectroscopy. The assistance of U. Rosowski in the maintenance of the H maser and data analysis has been important. C. Wellers and V. Vogt contributed in obtaining and characterizing the OPO. M. G. Hansen and I. V. Kortunov are acknowledged for their help on setting up the locking and metrology scheme of the OPO. We also thank E. Wiens for support in the optical frequency measurements. We thank S. Sturm, F. Heiße, C. König and S. Ulmer for discussions about the CPT tests. This work has received funding from the European Research Council under the European Union's Horizon 2020 research and innovation programme (Grant Agreement No. 786306, PREMOL (S.S.)) and from both the German Research Foundation and the state of North-Rhine-Westphalia (Grant Nos. INST-208/774-1 FUGG (S.S.) and INST-208/796-1 FUGG (S.S.)).

Author contributions

M.R.S. and S.A. performed the experiments and analysed the data. M.R.S. developed and characterized the spectroscopy laser system. S.A. maintained the apparatus. S.S. conceived the experiment, supervised the project and performed analyses. All authors contributed to writing the manuscript and reviewing the data.

Competing interests

The authors declare no competing interests.

Additional information

Extended data is available for this paper at https://doi.org/10.1038/s41567-023-02320-z.

Supplementary information The online version contains supplementary material available at https://doi.org/10.1038/s41567-023-02320-z.

Correspondence and requests for materials should be addressed to S. Schiller.

Peer review information *Nature Physics* thanks Shui-Ming Hu, Krzysztof Pachucki and Xin Tong for their contribution to the peer review of this work.

https://doi.org/10.1038/s41567-023-02320-z

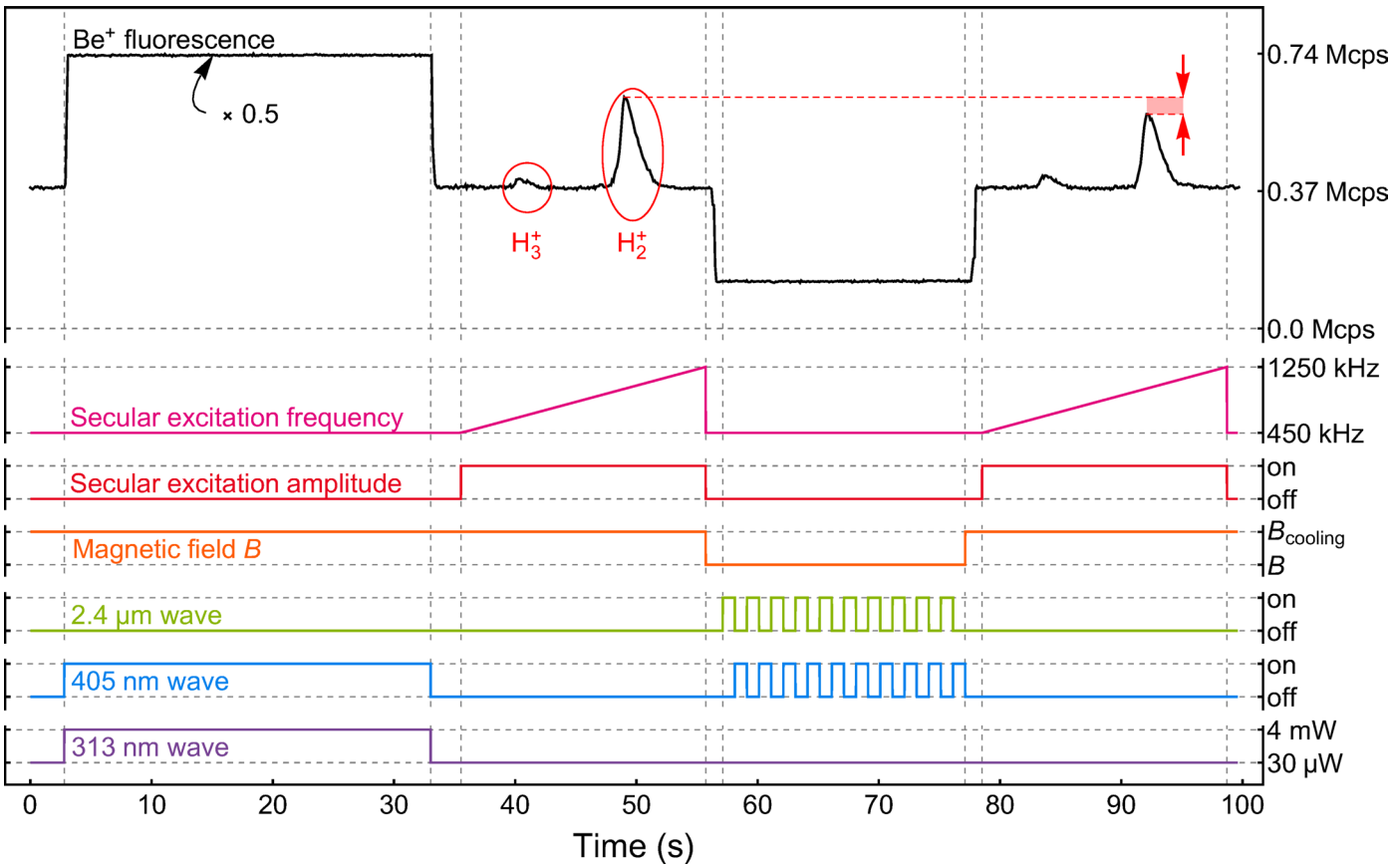

Extended Data Fig. 1 | The H_2^+ spectroscopy cycle. The black trace is the Be^+ fluorescence detected by a photomultiplier tube in mega counts per second (Mcps). During the depletion of the excited state population (see Methods, section 1.a), the fluorescence is multiplied by 0.5 for illustration purposes. The red ovals indicate the radial secular excitation resonance of the trapped H_2^+ and H_3^+ ions. The actual spectroscopy signal, that is the reduction of the number of trapped H_2^+ ions by the REMPD process, is highlighted in the top (black) signal by the red dashed lines and red arrows. The interleaved shuttering during the REMPD is shown simplified with only 10 repetitions. In actuality, there are 310 repetitions of duration ≃ 62 ms each. Each consists of two 30 ms and two 1 ms intervals. During the 30 ms intervals, either the 2.4 μm wave or the 405 nm wave is sent to the ions. The 1 ms intervals act as a buffers in-between. The cycle for measuring the background is analogous, except that the 2.4 μm wave is off during the whole cycle. During the exposure to the REMPD lasers, the magnetic field was $|B| \leq 0.2\,\mu$T, while at all other times a magnetic field B_{cooling} for the purpose of Doppler-cooling was applied. The values and status of each parameter are displayed on the right-hand vertical axis.

https://doi.org/10.1038/s41567-023-02320-z

Extended Data Table 1 | Hamiltonians for rovibrational levels (v, N=0, 2) in H_2^+

m_F	$H_{spin}(N=0)/c_e$	$H_{Zeeman}(N=0, m_F)/b$
$-\frac{1}{2}$	(0)	$\frac{1}{2}(g_e)$
$\frac{1}{2}$	(0)	$\frac{1}{2}(-g_e)$

m_F	$H_{spin}(N=2)/c_e$	$H_{Zeeman}(N=2, m_F)/b$
$-\frac{5}{2}$	1	$\frac{1}{2}(g_e+4g_1)$
$-\frac{3}{2}$	$\begin{pmatrix} -\frac{3}{2} & 0 \\ 0 & 1 \end{pmatrix}$	$\frac{1}{10}\begin{pmatrix} -3(g_e-6g_1) & 4(g_e-g_1) \\ 4(g_e-g_1) & 3(g_e+4g_1) \end{pmatrix}$
$-\frac{1}{2}$	$\begin{pmatrix} -\frac{3}{2} & 0 \\ 0 & 1 \end{pmatrix}$	$\frac{1}{10}\begin{pmatrix} -g_e+6g_1 & 2\sqrt{6}(g_e-g_1) \\ 2\sqrt{6}(g_e-g_1) & g_e+4g_1 \end{pmatrix}$
$\frac{1}{2}$	$\begin{pmatrix} -\frac{3}{2} & 0 \\ 0 & 1 \end{pmatrix}$	$\frac{1}{10}\begin{pmatrix} g_e-6g_1 & 2\sqrt{6}(g_e-g_1) \\ 2\sqrt{6}(g_e-g_1) & -g_e-4g_1 \end{pmatrix}$
$\frac{3}{2}$	$\begin{pmatrix} -\frac{3}{2} & 0 \\ 0 & 1 \end{pmatrix}$	$\frac{1}{10}\begin{pmatrix} 3(g_e-6g_1) & 4(g_e-g_1) \\ 4(g_e-g_1) & -3(g_e+4g_1) \end{pmatrix}$
$\frac{5}{2}$	1	$\frac{1}{2}(-g_e-4g_1)$

H_{spin} is the hyperfine structure hamiltonian. The Zeeman hamiltonian H_{Zeeman} for N=2 levels is approximate. Here, $c_e(v,N)$ is the spin-rotation coefficient, m_F is the projection of the total angular momentum F onto the static magnetic field direction, $g_e(v,N)$ and $g_I(v,N)$ are the electron and rotational g factors, respectively, and $b=\mu_B B=e\hbar B/2m_e$ is the product of Bohr magneton μ_B and magnetic field B, expressed in Hz, with the electron charge e, the reduced Planck constant $\hbar$, and the electron mass m_e. Note that $g_e \simeq -2$ is negative.

https://doi.org/10.1038/s41567-023-02320-z

Extended Data Table 2 | Approximate expressions for the energies of the states of H_2^+ in rotational levels N=2

	Small-B expansion	
m_F	lower energy group, F=3/2	higher energy group, F=5/2
$-\frac{5}{2}$		$c_e + \frac{1}{2} b (g_e + 4 g_1)$
$-\frac{3}{2}$	$-\frac{3 c_e}{2} - \frac{3}{10} b (g_e - 6 g_1) - \frac{8 b^2 (g_e-g_1)^2}{125 c_e}$	$c_e + \frac{8 b^2 (g_e-g_1)^2}{125 c_e} + \frac{3}{10} b (g_e + 4 g_1)$
$-\frac{1}{2}$	$-\frac{3 c_e}{2} - \frac{1}{10} b (g_e - 6 g_1) - \frac{12 b^2 (g_e-g_1)^2}{125 c_e}$	$c_e + \frac{12 b^2 (g_e-g_1)^2}{125 c_e} + \frac{1}{10} b (g_e + 4 g_1)$
$\frac{1}{2}$	$-\frac{3 c_e}{2} + \frac{1}{10} b (g_e - 6 g_1) - \frac{12 b^2 (g_e-g_1)^2}{125 c_e}$	$c_e + \frac{12 b^2 (g_e-g_1)^2}{125 c_e} - \frac{1}{10} b (g_e + 4 g_1)$
$\frac{3}{2}$	$-\frac{3 c_e}{2} + \frac{3}{10} b (g_e - 6 g_1) - \frac{8 b^2 (g_e-g_1)^2}{125 c_e}$	$c_e + \frac{8 b^2 (g_e-g_1)^2}{125 c_e} - \frac{3}{10} b (g_e + 4 g_1)$
$\frac{5}{2}$		$c_e - \frac{1}{2} b (g_e + 4 g_1)$

	Large-B expansion	
m_F	lower energy group, m_s=-1/2	higher energy group, m_s=1/2
$-\frac{5}{2}$	$c_e + \frac{1}{2} b (g_e + 4 g_1)$	
$-\frac{3}{2}$	$\frac{c_e}{2} + \frac{c_e^2}{b (g_e-g_1)} + \frac{1}{2} b (g_e + 2 g_1)$	$-c_e - \frac{c_e^2}{b (g_e-g_1)} + \frac{1}{2} b (-g_e + 4 g_1)$
$-\frac{1}{2}$	$\frac{b g_e}{2} + \frac{3 c_e^2}{2 b (g_e-g_1)}$	$-\frac{c_e}{2} - \frac{3 c_e^2}{2 b (g_e-g_1)} + \frac{1}{2} b (-g_e + 2 g_1)$
$\frac{1}{2}$	$-\frac{c_e}{2} + \frac{1}{2} b (g_e - 2 g_1) + \frac{3 c_e^2}{2 b (g_e-g_1)}$	$-\frac{b g_e}{2} - \frac{3 c_e^2}{2 b (g_e-g_1)}$
$\frac{3}{2}$	$-c_e + \frac{1}{2} b (g_e - 4 g_1) + \frac{c_e^2}{b (g_e-g_1)}$	$\frac{c_e}{2} + \frac{1}{2} b (-g_e - 2 g_1) - \frac{c_e^2}{b (g_e-g_1)}$
$\frac{5}{2}$		$c_e - \frac{1}{2} b (g_e + 4 g_1)$

Here, $c_e(v,N)$ is the spin-rotation coefficient, m_F is the projection of the total angular momentum F onto the static magnetic field direction, $g_e(v,N)$ and $g_l(v,N)$ are the electron and rotational g factors, respectively, m_s is the electron spin projection quantum number and $b=\mu_B B=e\hbar B/2m_e$ is the product of Bohr magneton μ_B and magnetic field B, expressed in Hz, with the electron charge e, the reduced Planck constant $\hbar$, and the electron mass m_e. Note that $g_e \simeq -2$ is negative.

https://doi.org/10.1038/s41567-023-02320-z

Extended Data Table 3 | Theoretical values of the spin and Zeeman contributions of some Zeeman components of the studied transition (v=1, N=0)→(v'=3, N'=2), in weak magnetic field B in units of μT

HFS component					contributions	
	F	m_F	F'	$m_{F'}$	spin frequency (kHz)	Zeeman shift
$f_a^{(-)}$	$\frac{1}{2}$	$-\frac{1}{2}$	$\frac{5}{2}$	$-\frac{5}{2}$	34 730.3	$+14\,\mathrm{Hz}\times B$
$f_a^{(+)}$	$\frac{1}{2}$	$+\frac{1}{2}$	$\frac{5}{2}$	$+\frac{5}{2}$	34 730.3	$-14\,\mathrm{Hz}\times B$
$f_b^{(-)}$	$\frac{1}{2}$	$+\frac{1}{2}$	$\frac{3}{2}$	$-\frac{3}{2}$	−52 095.4	$-5.6\,\mathrm{kHz}\times B-1.4\,\mathrm{Hz}\times B^2$
$f_b^{(+)}$	$\frac{1}{2}$	$-\frac{1}{2}$	$\frac{3}{2}$	$+\frac{3}{2}$	−52 095.4	$+5.6\,\mathrm{kHz}\times B-1.4\,\mathrm{Hz}\times B^2$
$f_{\mathrm{spin-avg}}$	$\frac{3}{10}(f_a^{(-)}+f_a^{(+)})+\frac{2}{10}(f_b^{(-)}+f_b^{(+)})$				0	$-0.6\,\mathrm{Hz}\times B^2$
c_e	$\frac{1}{5}(f_a^{(-)}+f_a^{(+)})-\frac{1}{5}(f_b^{(-)}+f_b^{(+)})$				34 730.3	$+0.6\,\mathrm{Hz}\times B^2$

Values are rounded. In future spectroscopy with Doppler-free resolution, the four frequencies $f_{a,b}^{(+,-)}$ should be measured in order to obtain $f_{\mathrm{spin-avg}}$ as shown in row 7. The linear Zeeman shifts cancel in the computed $f_{\mathrm{spin-avg}}$ and also in the computed spin-rotation interaction strength c_e, leaving small nonzero quadratic shifts. Here, $m_F(m_F')$ is the projection of the total angular momentum $F(F')$ of the lower (upper) state onto the static magnetic field direction.